# Structural and electronic properties of rare earth silicide nanowires on Si(557)

Martina Wanke, Karolin Löser, Gerhard Pruskil, and Mario Dähne*
*Institut für Festkörperphysik, Technische Universität Berlin, Hardenbergstraße 36, D-10623 Berlin, Germany*
(Received 27 October 2008; revised manuscript received 20 February 2009; published 16 April 2009)

We report on the atomic structure and electronic properties of self-organized dysprosium and erbium silicide nanowires on Si(557), studied using scanning tunneling microcopy and angle-resolved photoelectron spectroscopy. The nanowires were prepared by deposition of different rare earth amounts and subsequent annealing for silicide formation. Due to the stepped structure of the Si(557) surface, nanowires form along the step edges, showing a variety of structurally and electronically different types, depending on the preparation conditions. At submonolayer dysprosium coverages, different chainlike structures dominate, showing one-dimensional dispersion with half-metallic properties. These nanowire regions are separated by $7\times7$ reconstructed Si(111) facets or submonolayer dysprosium silicide patches on these facets. At monolayer coverages, in contrast, mainly nanowires with lengths exceeding 1 $\mu$m and widths of a few nanometers are found, forming on the (111) facets of the Si(557) surface. Their electronic properties are characterized by a two-dimensional band structure with strong dispersion both parallel and perpendicular to the nanowires and clear metallic behavior, and it is demonstrated that they are formed from hexagonal $DySi_2$ monolayers. In the case of thicker silicide layers, metallic nanowires form again on the Si(111) facets, but with clear structural and electronic characteristics of hexagonal $Dy_3Si_5$ multilayers. At these coverages, additional structures are found, which show an intense signal in the photoelectron spectroscopy data. Related experiments on the growth of erbium silicides indicated the formation of very similar nanowire structures.

DOI: 10.1103/PhysRevB.79.155428 PACS number(s): 81.07.Vb, 73.21.Hb, 68.37.Ef, 79.60.Jv

## I. INTRODUCTION

Nanostructures are of high interest because of the quantum effects due to the nanometer scale, which result in physical properties tunable by size and shape, allowing a variety of applications, e.g., in electronic devices. For the preparation of nanostructures, self-assembly is one of the most powerful tools both to overcome the resolution limits of traditional lithographic techniques and for reducing the amount of crystalline defects, which may deteriorate the electronic and optoelectronic properties. In this respect, self-organized nanowires are interesting both for an improved understanding of the growth mechanisms and because of the peculiar physical and in particular electronic properties of these one-dimensional structures. Furthermore, they are attractive, e.g., for the fabrication of electronic devices or for high-density data storage.

About one decade ago it was demonstrated that self-organized rare earth silicide nanowires can be grown on planar Si(001)$2\times1$ surfaces,[1] and since then several studies were performed to study growth, structure, and electronic properties on both planar and vicinal Si(001)$2\times1$ surfaces.[2–8] The structural properties of these nanowires were shown to depend strongly on the preparation conditions, notably rare earth coverage and substrate temperature during deposition or post-growth annealing. One species dominant at monolayer coverages, the so-called broad nanowires, was shown to consist of hexagonal rare earth disilicide such as $DySi_2$ with its $c$ axis aligned perpendicular to the nanowires but within the surface plane.[3,4] These nanowires are forming due to anisotropic strain, which is negligible in nanowire direction but considerable in $c$ direction. Recently it was demonstrated that these nanowires are metallic and characterized by a one-dimensional electronic structure with a strong dispersion in nanowires direction but negligible dispersion in perpendicular direction.[5,6]

The nanowire growth on Si(001) is in strong contrast to the layered growth of rare earth silicides found on planar Si(111). In the latter case, the trivalent rare-earth metals are forming silicides with wide defect-free terraces[9] and rather extreme Schottky-barrier heights.[10–12] In the case of monolayer coverages, almost unstrained rare earth disilicides with the $c$ axis normal to the substrate surface are observed,[13] which are metallic and characterized by a two-dimensional electronic structure.[14,15] In the case of thicker layers, the disilicide is slightly modified due to an ordered arrangement of silicon vacancies in the planar graphenelike silicon sheets located in the silicide bulk, resulting in a $\sqrt{3}\times\sqrt{3}$R30° superstructure with—for the case of dysprosium—a $Dy_3Si_5$ composition.[13] On vicinal Si(111) surfaces with high miscut angles, rare earth silicide growth was observed as well, but in this case arranged in the form of silicide nanowires along the step edges.[16]

The latter result indicates that self-organized nanowire growth can also be expected for the Si(557) surface. Si(557) is vicinal to Si(111) by an angle of about 10°, and the bare surface facets into (111) terraces with widths of about 3 nm, separated by [112]-oriented regions of about the same width.[17–19] Up to now, only a few investigations were performed to study thin-film growth on the Si(557) surface. Mainly the formation of Au chains[20–22] and Pb nanowires[23] on Si(557) was studied in detail. In the case of the Au chains, an anisotropic electronic structure was observed, which, however, did not show a pure one-dimensional behavior since weak interactions of neighboring nanowires lead to a weak dispersion perpendicular to the nanowires.[22] For Pb nanowires, a temperature-dependent switching of the dimensionality could be observed.[23] Rare earth silicide structures

 

on the Si(557) surface, however, were—to our knowledge—not investigated, with the exception of a recent publication, where we briefly reported on the properties of dysprosium silicide nanowires at monolayer coverages.[24]

In this work we present a detailed study on the formation of different wirelike rare earth silicide structures on the Si(557) surface in a large range of exposures and post-growth annealing conditions. The use of scanning tunneling microcopy (STM) and angle-resolved photoelectron spectroscopy (ARPES) provides both structural information and $\vec{k}$-resolved data on the electronic properties, respectively. Depending on the preparation conditions, different structures with different dimensionality of the electronic properties are found. Submonolayer dysprosium coverages lead to chainlike structures with clearly one-dimensional electronic properties and half-metallic behavior. At coverages around one monolayer, in contrast, rather broad nanowire structures were formed on the (111) facets of the Si(557) surface, which show both structural characteristics and the two-dimensional electronic properties of metallic hexagonal $DySi_2$ monolayers on Si(111). The situation is similar at thicker layers, where predominantly hexagonal $Dy_3Si_5$ multilayers are formed on the (111) facets, but here also other structures seem to contribute. STM and ARPES data of erbium silicides on Si(557) show essentially a very similar behavior.

## II. EXPERIMENTAL DETAILS

Clean Si(557) surfaces were prepared in the usual way[26] by repeated flashing a resistively heated *p*-doped Si(557) wafer to 1100–1200 °C and then cooling down, which occurred slowly during about 5 min within the temperatures range from 800 °C to 500 °C in order to allow the formation of the facetted surface structure. The sample temperatures were measured using an infrared pyrometer with an accuracy of ±20 °C.

The rare earth silicide structures were prepared *in situ* by deposition of 99.9% pure dysprosium or erbium from electron-beam heated tungsten crucibles on the substrate held at room temperature. The amount of rare earth exposure was determined by using a quartz-crystal microbalance with an accuracy of 20%. Afterwards the sample was annealed for about 2 min for silicide formation, resulting in different nanowire types depending on the rare earth exposure and post-growth annealing temperature.

For the STM experiments we used a noncommercial setup with tunneling currents from 0.1 to 0.5 nA and sample voltages between −1 and −2.5 V, i.e., the filled states mostly related to the silicon atoms were imaged.[13] The ARPES experiments were performed at the BUS beamline (U125/2-SGM) at BESSY II in Berlin using a Scienta SES 100 spectrometer at a photon energy of 41 eV. The base pressure in both systems was lower than $5\times10^{-11}$ mbar and did not exceed $2\times10^{-10}$ mbar during the entire preparation process. It should be noted that such excellent ultrahigh-vacuum conditions are necessary in order to prevent contamination of the highly reactive rare earth systems.

## III. RESULTS AND DISCUSSION

### A. Bare Si(557) surface

In Fig. 1, representative STM results are shown for the

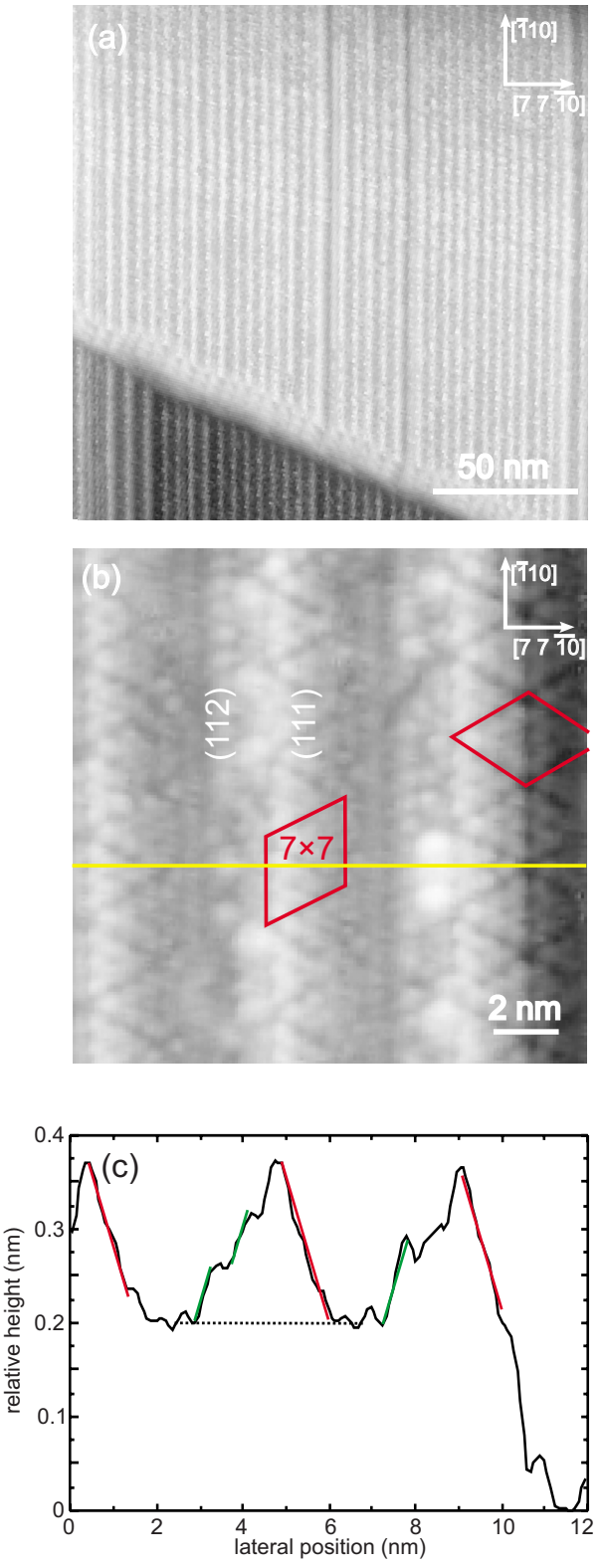


FIG. 1. (Color online) (a) STM overview image and (b) detailed image of the bare Si(557) surface, with the $7\times7$ unit cell marked by red rhombi. (c) Height profile (black) along the yellow line in (b) to determine the facet orientations. The red lines indicate facets with an angle of about 10° with respect to the average (557) surface (dotted black line), typical for (111) facets, while the green lines with an angle of about −10° can be related to (112) facets.

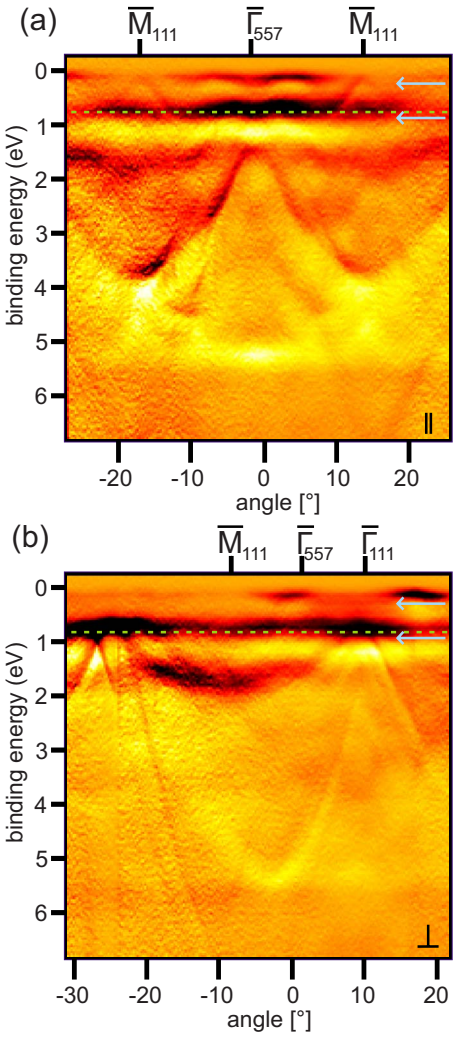


FIG. 2. (Color online) ARPES data of the bare Si(557) surface taken (a) along and (b) perpendicular to the steps in $[1\bar{1}0]$ direction, which separate the facets.

bare Si(557) surface. It is clearly observed in Fig. 1(a) that the surface forms regular facets with steps along the $[1\bar{1}0]$ direction. Another high straight step is observed at the bottom of the image, which is related to a slight misorientation of the silicon wafer. As shown in Fig. 1(b), one facet family consists of (111) terraces with $7\times7$ (and sometimes also $5\times5$, not shown here) reconstructed patches and widths of one to two $7\times7$ unit cells amounting in average to about 3 nm.[17] As derived from the height profile shown in Fig. 1(c), also the angle of these terraces (indicated by the red lines), amounting to about 10° with respect to the average substrate surface (black dotted line), agrees nicely with the (111) orientation. The other facet family (green lines) also shows atomic resolution and can be assigned to a stepped Si(112) surface on the basis of the measured angle of about −10° with respect to the average surface. These findings are in agreement with earlier STM results on this surface.[17–19]

Figure 2 shows corresponding ARPES results of the bare Si(557) surface (a) along and (b) perpendicular to the steps. These plots show the photoelectron intensity as a function of binding energy and angle and thus directly visualize the dispersion of the electronic states in the tilt direction of the analyzer with respect to the sample. The ARPES data are filtered using illumination effects in order to highlight the dispersing features. Here and in the following, $\bar{M}_{111}$ and $\bar{\Gamma}_{111}$ represent the symmetry points in the surface Brillouin zone of the (111) facets, while $\bar{\Gamma}_{557}$ stands for the surface normal.

At binding energies of 0.2 and 0.8 eV, the typical nondispersing surface states of the Si(111)$7\times7$ surface are found,[25] which are marked by blue arrows. At about 0.7 eV binding energy there is a step in the photoelectron intensity, marked by dashed green lines, which can be related to the bulk valence-band maximum, in nice agreement with Ref. 25.

There are further strongly dispersing states at higher binding energies, which are mainly related to silicon bulk bands and will thus not be discussed here. In the following, only bands within the substrate band gap will be considered, i.e., with binding energies up to about 0.7 eV, since they clearly belong to the silicon surface and/or the deposited silicide nanostructures.

### B. Submonolayer dysprosium coverages

Now we discuss the structural and electronic properties observed at low Dy exposures. At submonolayer Dy coverages of 0.5–1 Å, various linear structures are observed by STM, as shown in Fig. 3. These structures have some similarities with the so-called thin nanowires observed on Si(001).[26,27] As it is shown in Fig. 3(b), they usually consist of thin linelike features with only minute corrugation in nanowire direction and atomic chains in between with strong corrugation, but also fractions of this structure are observed. Both linelike and chainlike features show a 0.76 nm periodicity in nanowire direction, corresponding to two lattice vectors of the Si substrate in $[1\bar{1}0]$ direction. The typical width of the entire nanowire structure amounts to about 2 nm. The nanowires form a rather periodic lattice with a lattice constant perpendicular to the nanowires of about 3 nm.

In Fig. 3(a), an inclined stripe showing the Si(111)$7\times7$ reconstruction is visible in between the chainlike nanowires. In contrast, Fig. 3(b) shows a similar inclined stripe with a periodic structure different from Si(111)$7\times7$. A closer analysis shows windmill-like triple protrusions (orange arrow) with a periodicity of about 1.2 nm on several nanometer wide patches separated by linear dislocations. These structural features are typical for a silicide found on Si(111) formed from half a monolayer of dysprosium, which is characterized by a $2\sqrt{3}\times2\sqrt{3}$ superstructure.[13]

The height contour across the nanowires shown in Fig. 3(c) shows the characteristic angle of about 10° between the (111) facets (red line) and the average surface (black dotted line), as already expected. Furthermore, the green line marks the orientation of the nanowire facet, which has an angle of about −2° to the average surface orientation, indicating that the nanowires grow on facets different from (557). This behavior demonstrates that the initial faceting of the bare Si(557) is not conserved when the chainlike nanowires are formed. The formation of wide non-(557) facets indicates a high thermodynamic stability of this submonolayer nanowire

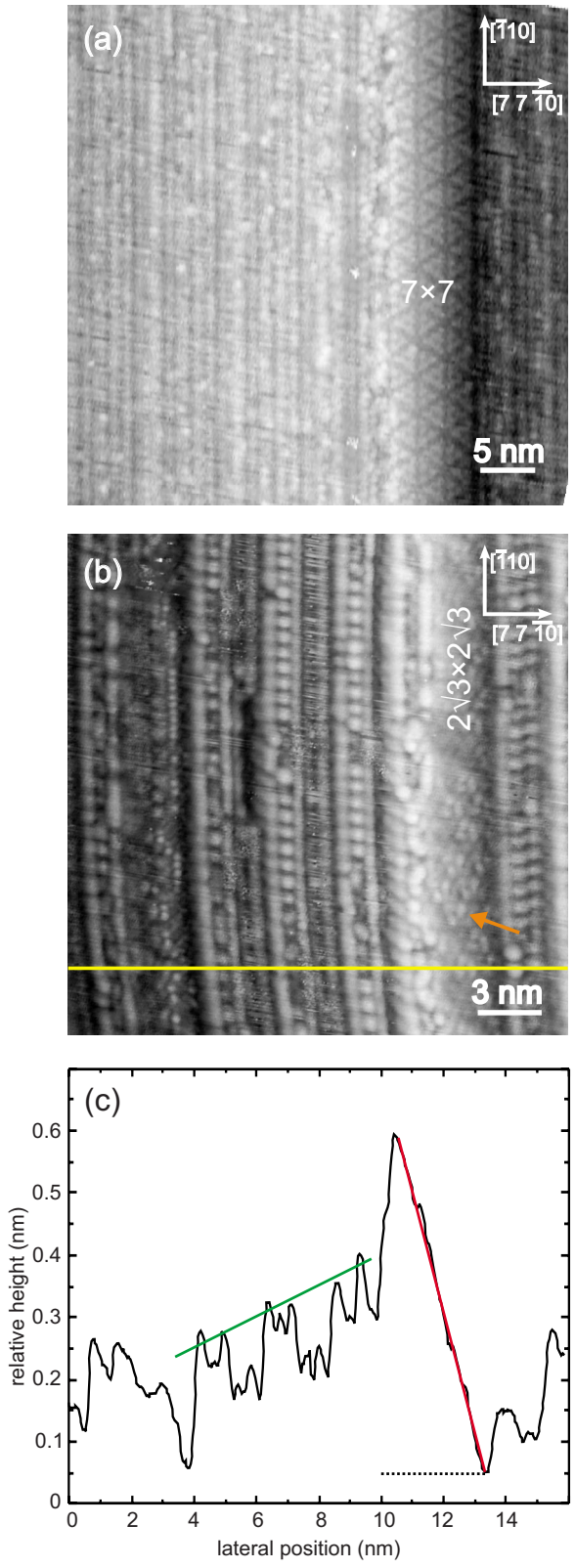


FIG. 3. (Color online) STM images of submonolayer nanowire structures on Si(557) prepared (a) with 0.5 Å Dy and an annealing temperature of 650 °C and (b) with 1 Å Dy and 700 °C, and (c) height contour along the yellow line in (b). In (a) and (b) also (111) terraces are found with different appearances.

structure, which, however, also requires extended (111) facets in order to compensate the misalignment of the nanowire facets with respect to the average (557) surface.

Unfortunately, the present STM data do not allow the development of a structure model for the thin nanowires on Si(557). This is attributed to the large unit cell as well as the stepped substrate surface, resulting in a rather complicated structure. In addition, up to now high-resolution STM images could not be obtained at positive voltages, where dysprosium-related features are pronounced. However, there are some indications for certain structural building blocks. First, dysprosium atoms may be found inside of silicon cages because of the surplus of silicon during silicide formation, as already found for the broad nanowires on Si(001). Second, also dysprosium atoms directly at the surface, such as in the $2\sqrt{3}\times 2\sqrt{3}$ superstructure on the Si(111) facets,[13] cannot be excluded since this structure is also stable at high temperatures up to 700 °C, as observed in Fig. 3(b). Third, according to the structural model for the thin nanowires on Si(001) (Ref. 26) the different corrugation amplitudes of the atomic chains and the linelike features could be related to different orientations of Si dimers on top of the silicide. Hence, these three building blocks could contribute to a structural model.

The typical electronic structure of the chainlike nanowires prepared at submonolayer coverages is shown in Fig. 4. It is characterized by a band with strong dispersion parallel to the nanowires with a holelike state just reaching the Fermi energy at the $\bar{J}$ point located at off-normal angles [arrows in Fig. 4(a)]. From the curvature of this band at $\bar{J}$, the effective mass can be determined to about $0.13m_e$, with $m_e$ being the free-electron mass. Perpendicular to the nanowires, in contrast, no dispersion is observed [Fig. 4(b)] since the experimental band width including the experimental uncertainty is well below 0.2 eV.

The observed spectral features close to the Fermi energy differ strongly from the surface states of the bare Si(111)7 $\times$7 surface shown in Fig. 2, so that they can be related to the nanowires. The typical surface-state emission of Si(111)7 $\times$7 is also expected to be very weak because of the small fraction of the surface corresponding to (111) facets. In addition, the features cannot result from the $2\sqrt{3}\times 2\sqrt{3}$ structure on the (111) facets, which would show a two-dimensional band structure. Thus it may be concluded that the nanowires have a practically one-dimensional electronic structure with half-metallic behavior in nanowire direction and only negligible coupling of the electronic states from neighboring nanowires.

It should be noted here that such holelike parabolic bands close to the Fermi energy were already observed in the case of the bare Si(557) surface, as shown in Fig. 2(a), but with an extremely low intensity. In principle they could be related to step-induced surface states of Si(557) if such a structural unit would also be present in the submonolayer case. However, the much higher intensity of this feature in the present case makes this assignment improbable. Thus it cannot be excluded that small amounts of dysprosium stay on the surface even after flashing since this wafer had already been exposed to dysprosium before preparation of the bare Si(557) surface. This could result in a weak nanowire related signal in Fig. 2(a).

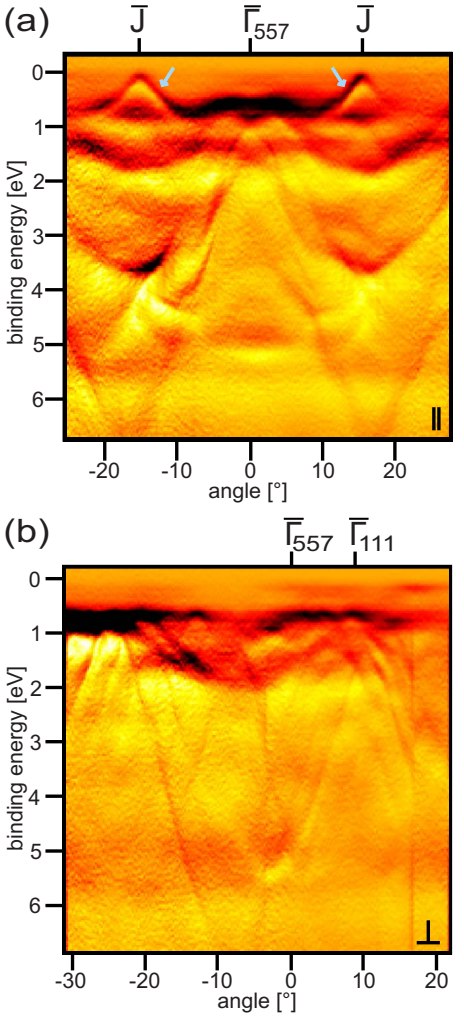


FIG. 4. (Color online) ARPES data of the chainlike nanowire structure on Si(557) prepared with 0.5 Å Dy and an annealing temperature of 700 °C, taken (a) along and (b) perpendicular to the nanowires.

Parallel to the nanowires, the electronic states reach the Fermi energy at the $\bar{J}$ points. These angles of high symmetry correspond to the boundary of the Brillouin zone of a structure with 0.38 nm periodicity, indicating that no influence of the double periodicity observed by STM is found in the ARPES data. This behavior can be discussed in the framework of the structure of the thin nanowires on Si(001),[26] which probably consists of similar building blocks as the present structure. This structure contains dysprosium chains surrounded by a silicon cage structure with 0.38 nm periodicity, while the surface is characterized by silicon surface dimers with 0.76 nm periodicity. Thus it can be assumed for the present case that the main features in the observed electronic structure and in particular the half-metallicity in nanowire direction can be related to the dysprosium atoms and to those silicon atoms, which are located underneath the surface and have 0.38 nm periodicity. In contrast, the silicon surface dimers—and other structural units with 0.76 nm periodicity—do not contribute significantly to the ARPES data, but dominate the appearance in the STM images.

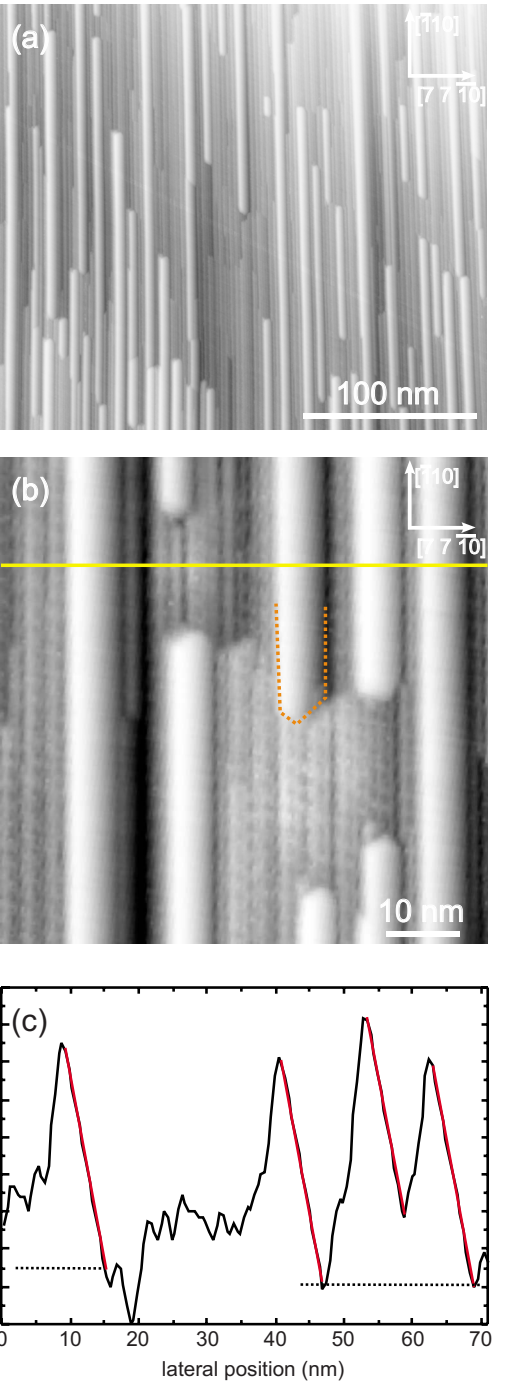


FIG. 5. (Color online) STM images of $DySi_2$ nanowires on Si(557) prepared with 2 Å Dy and an annealing temperature of 700 °C. (a) Shows an overview image of the nanowire growth on the sample surface, (b) a more detailed image, and (c) is a height contour along the yellow line in (b). The orange dotted lines in (b) indicate the endpieces of the nanowires with hexagonal shape characteristic for $DySi_2$ monolayers on Si(111).

### C. Monolayer dysprosium coverages

For coverages around 2 Å, i.e., close to one monolayer, different silicide nanowires grow along the $[1\bar{1}0]$ direction, as shown in Fig. 5. These so-called broad nanowires are characterized by widths of 3–5 nm and lengths exceeding

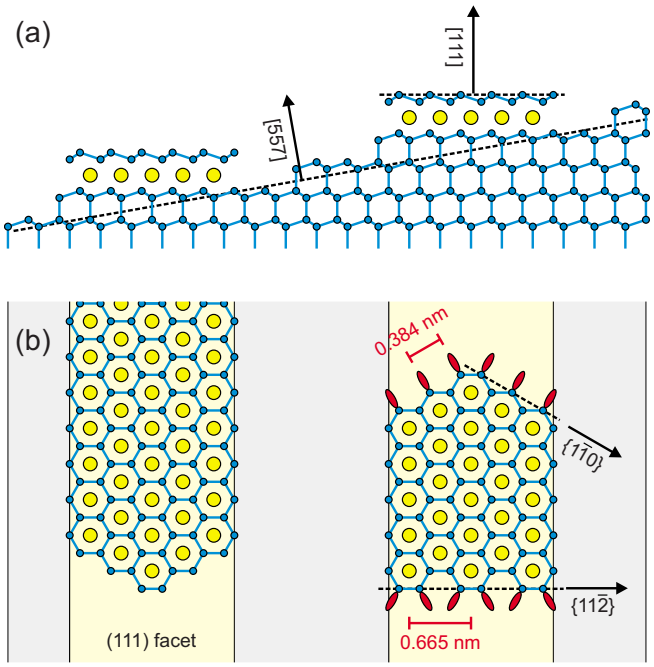


FIG. 6. (Color online) Schematic model of the silicide nanowires consisting of hexagonal $DySi_2$ monolayers on the (111) facets, (a) side view and (b) top view. The lateral dangling bonds of the surface silicon layer are indicated by red ellipses. In reality, the facets are wider than it is shown here.

1000 nm. In principle, the length of the nanowires is determined by the diffusion kinetics along the terraces and the amount of available dysprosium. Under optimum conditions, the length is only limited by the high substrate steps formed due to a misorientation of the substrate, as observed in Fig. 1. The area in between is covered by structures similar to the thin submonolayer nanowires discussed in Sec. III B.

The angle of about 10° between the surface of the broad nanowires and the average substrate orientation, as derived from the height contour in Fig. 5(c), indicates that these nanowires grow on the Si(111) terraces. Furthermore, they show hexagonal endpieces with clear straight edges along the {1$\bar{1}$0} directions, as indicated by the dotted lines in Fig. 5(b). These orientations of the edges are characteristic for hexagonal $DySi_2$ monolayer islands grown on Si(111) with their *c* axis in surface-normal direction.[15]

It will be demonstrated in the following that these nanowires prepared with monolayer dysprosium coverages in fact consist of hexagonal $DySi_2$ grown on the (111) facets since (a) their surface has the orientation of the (111) facets, (b) the structure of the endpieces agrees nicely with the edges of $DySi_2$ on Si(111), and (c) the band structure matches exactly that of the similar $ErSi_2$ monolayers on Si(111).

A schematic model for the growth of the $DySi_2$ structure on the (111) facets is shown in Fig. 6. The hexagonal *c* axis is normal to the Si(111) facets where the nanowires grow on. $DySi_2$ consists of a silicon bilayer at the surface and a dysprosium layer underneath. Such a growth of two-dimensional films, as it was observed for the planar (111) surface at monolayer exposures,[15] is also strongly favored in the present case because of the negligible lattice mismatch. However, growth is limited here to the width of the substrate terraces. Thus, in this case silicide nanowires form in a self-organized way without the influence of strain, in contrast to the nanowire growth on Si(001).

The formation of hexagonal endpieces, which is characteristic for the disilicide monolayers, can be attributed to the low density of lateral dangling bonds of the silicon surface bilayer at {1$\bar{1}$0}-oriented edges. As derived from Fig. 6(b), {1$\bar{1}$0}-oriented edges have a dangling-bond density of 1/0.384 nm=2.60/nm, in contrast, e.g., to {11$\bar{2}$}-oriented edges with a 15% larger dangling-bond density of 2/0.665 nm=3.01/nm.

It should be noted here that atomic resolution could generally not be achieved at the $DySi_2$ nanowire surfaces (and also not for the $Dy_3Si_5$ nanowires discussed in Sec. III D) since this would require rather low tunneling voltages of a few 100 mV.[13] At the present nanowire samples, however, the rather narrow silicide regions are too close to surface regions covered with submonolayer nanowires, where such tunneling conditions cannot be maintained. Thus the unavoidable thermal drift prevented an imaging of the nanowire surface at low voltages. Hence, no clear structural assignment is possible on the basis of the present STM data alone. However, the ARPES data shown in the following clearly demonstrate that the nanowires consist of hexagonal $DySi_2$ monolayers.

ARPES data of these nanowires for angular variations along and perpendicular to the nanowire direction are shown in Figs. 7(a) and 7(b), respectively. A strong energy dispersion is observed in both cases with bands crossing the Fermi energy, indicating a two-dimensional metallic band structure. The dispersion along the nanowires, as shown in Fig. 7(a), is characterized by parabolic bands crossing the Fermi energy at off-normal directions, while a wavy dispersion is found around the surface normal $\bar{\Gamma}_{557}$ at a binding energy of about 1 eV. The dispersion perpendicular to the nanowires, as shown in Fig. 7(b), is also characterized by parabolic bands around the Fermi energy. Here, the angle of highest symmetry of the dispersion (at $\bar{\Gamma}_{111}$) is tilted by about 10° away from the surface normal (at $\bar{\Gamma}_{557}$), in agreement with the nominal angle between the (111) facets and the average (557) surface, indicating that the observed electronic structure stems from overlayers grown on the (111) facets.

No significant additional bands are observed in Fig. 7. Only an almost negligible contribution is found from the half-metallic nanowires dominant at submonolayer coverages since in nanowire direction a small signal from the holelike parabolic dispersion is visible around $\bar{M}_{111}$ [corresponding to $\bar{J}$ in Fig. 4(a)], as marked by the arrows in Fig. 7(a). Such submonolayer nanowires are also observed in the STM data presented in Fig. 5(b). Furthermore, no features at different angles of high symmetry are found in Fig. 7(b), so that other facets—such as the (112) facet of the Si(557) surface—do not contribute significantly. This suggests that other facets are not covered by a dysprosium silicide.

In order to confirm the assignment of the nanowire structure to $DySi_2$ monolayers on Si(111) facets, our ARPES data are compared with previous experimental findings on the

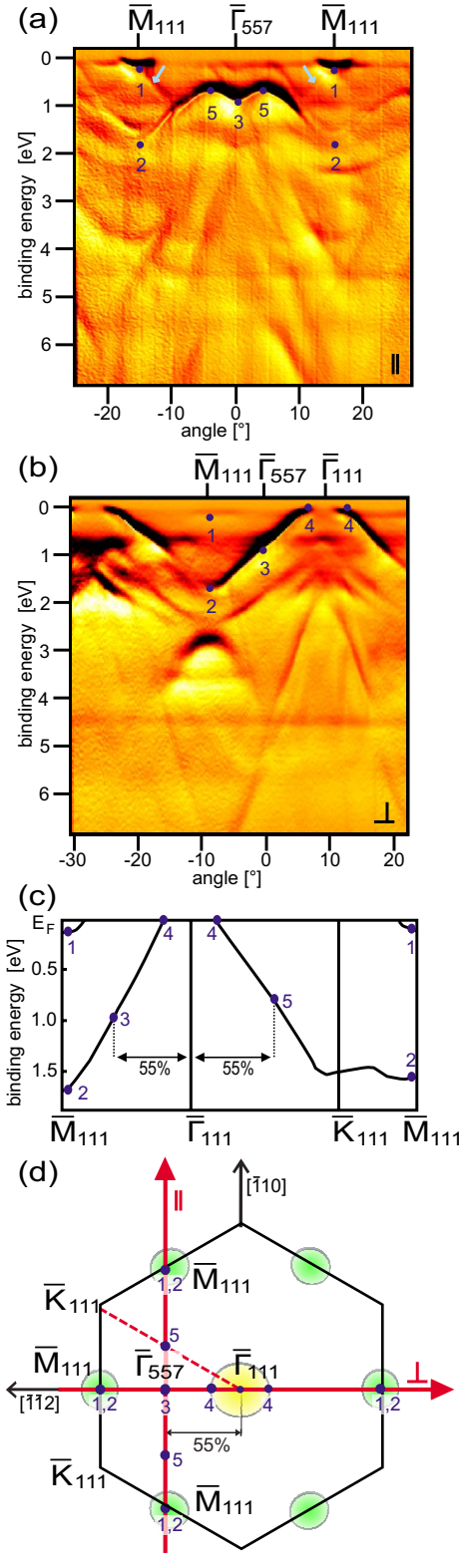


FIG. 7. (Color online) ARPES data (a) along and (b) perpendicular to the $DySi_2$ nanowires prepared with 2 Å Dy and an annealing temperature of 700 °C. The blue dots mark points of high symmetry in the ARPES data. The horizontal lines at around 4.5 and 5.5 eV binding energy stem from the Dy-4*f* emission. (c) Band structure of $ErSi_2$ on Si(111) from Refs. 14 and 15 for comparison. (d) Surface Brillouin zone of $DySi_2$ showing the directions of the measurements by red arrows.

electronic properties of the $ErSi_2$/Si(111) system,[14,15] which are shown in Fig. 7(c). Since $ErSi_2$ and $DySi_2$ monolayers on Si(111) are structurally and chemically identical,[13] also their electronic properties are expected to be very similar. In Fig. 7(d), the surface Brillouin zone of $DySi_2$/Si(111) is shown with electron pockets around $\bar{M}_{111}$ and a hole pocket around $\bar{\Gamma}_{111}$, as reported in Refs. 14 and 15 for $ErSi_2$/Si(111). It should be noted here that experimental constraints only allowed us to tilt the sample away from the surface normal corresponding to $\bar{\Gamma}_{557}$, which lies 55% away from the $\bar{\Gamma}_{111}$ point on the way to the $\bar{M}_{111}$ point at the used photon energy of 41 eV. Thus our data were taken along the red arrows marked by ∥ and ⊥ in Fig. 7(d).

A detailed analysis shows an excellent agreement of our data taken along both directions with the reported $ErSi_2$/Si(111) band structure. This is manifested in particular by the blue markers labeled 1 to 5. At marker 1, the electron pockets of the $\bar{M}_{111}$ point can be clearly identified in Figs. 7(a) and 7(b). At the $\bar{M}_{111}$ point there is a second dispersion curve at around 1.7 eV binding energy (marker 2). This curve will reach the Fermi energy at the hole pocket around the $\bar{\Gamma}_{111}$ point (marker 4). Marker 3 is the $\bar{\Gamma}_{557}$ point, and marker 5 lies at 55% on the way from the $\bar{\Gamma}_{111}$ point to the $\bar{K}_{111}$ point.

Perpendicular to the nanowires, the agreement of our ARPES data shown in Fig. 7(b) with the dispersion along $\bar{\Gamma}_{111}$–$\bar{M}_{111}$ for $ErSi_2$ shown in Fig. 7(c) is obvious. Also the binding energies at the markers 1, 2, and 4 are nicely reproduced. Parallel to the nanowires, the angular scan shown in Fig. 7(a) goes through markers 3 and 5, leading to the wavy appearance around $\bar{\Gamma}_{557}$, and hits markers 1 and 2 at $\bar{M}_{111}$. Again, a nice agreement is obtained at these points with the results reported for $ErSi_2$/Si(111).

The different appearance of the minima of the parabolas at the $\bar{M}_{111}$ point (marker 1) in Figs. 7(a) and 7(b) can be related to an unavoidable sample misalignment in the order of 1°, resulting in a slight deviation of the actual angular scans from the red arrows in Fig. 7(d). In particular, this misalignment results in a strongly reduced signal at marker 1 in Fig. 7(b), where the electron pocket is only cut at its margin.

From the curvature of the states crossing the Fermi energy, the effective masses can be determined. At the electron pockets around the $\bar{M}_{111}$ point (marker 1) it amounts to about $0.5m_e$. At the hole pocket around $\bar{\Gamma}_{111}$ (marker 4), in contrast, the band maximum is unoccupied so that the dispersion has to be extrapolated, yielding an estimated value for the effective mass in the order of $0.8m_e$.

From the structural observations and the measured electronic dispersion in excellent agreement with the $ErSi_2$/Si(111) band structure, it can be concluded that the nanowires grow on the (111) facets forming $DySi_2$ monolayers, resulting in a metallic two-dimensional electronic band structure with sixfold symmetry.

### D. Multilayer dysprosium coverages

At larger coverages of 3 Å and above, characteristic for multilayer growth, similar nanowires are observed at the

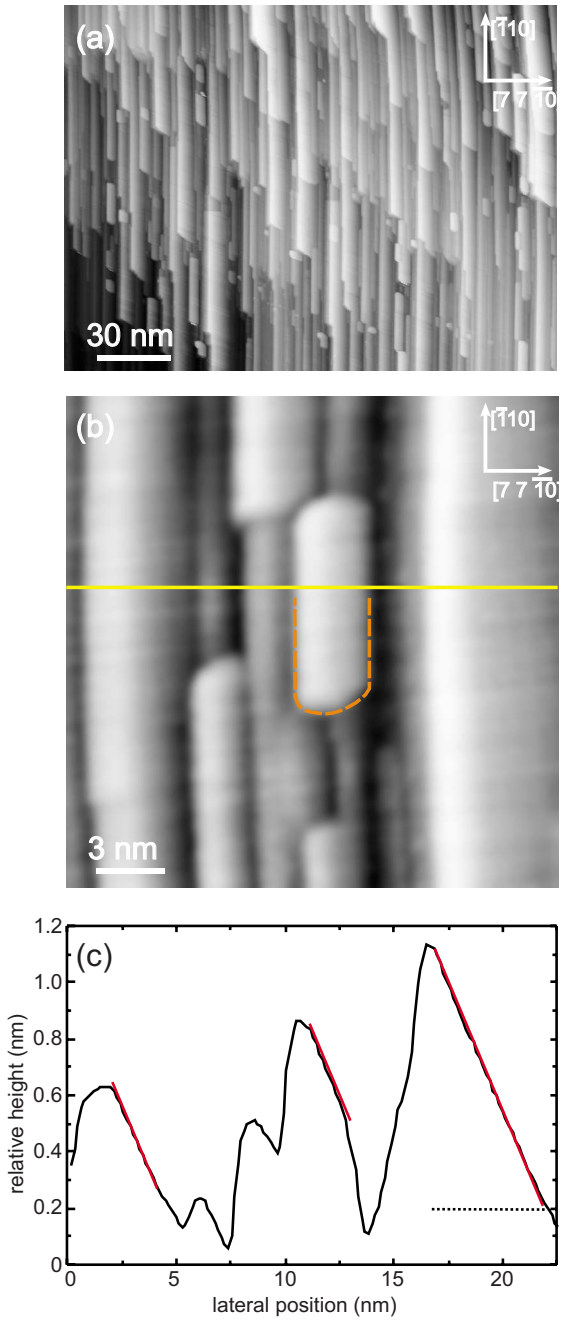


FIG. 8. (Color online) STM images of $Dy_3Si_5$ nanowires on Si(557) prepared with 3 Å Dy and an annealing temperature of 700 °C. (a) Shows an overview of the nanowire growth on the sample surface, (b) a more detailed image, and (c) is a height contour along the yellow line in (b). The orange dashed line in (b) indicates the endpieces of the nanowires with rounded shape characteristic for $Dy_3Si_5$ multilayers on Si(111).

(111) facets, as shown in Fig. 8. They appear slightly broader and denser than the monolayer-type nanowires described above. Furthermore, the endpieces are rounder than in the monolayer case, as indicated by the dashed line. Such endpieces are characteristic for the $Dy_3Si_5$ multilayer structure on Si(111),[13] which was found to form rather round terraces. This structural assignment is in agreement with recent transmission electron microscopy data on dysprosium silicide nanowires grown on vicinal Si(111) with higher miscut angles of 12° and 15°.[16]

In the $Dy_3Si_5$ compound, the silicide bulk consists of defective graphenelike Si sheets characterized by an ordered array of silicon vacancies, separated by dysprosium layers. Because of this vacancy structure, the density of dangling bonds does not seem to vary much with the orientation of the edge.[13] Accordingly the energy of the different edge orientations may be similar so that the $\{1\bar{1}0\}$ orientation is not favored any more. This holds in particular for the case of thicker nanowires, where the surface does not dominate any more, resulting in a rounder appearance of the endpieces.

In order to control if the nanowires actually consist of hexagonal $Dy_3Si_5$, representative ARPES results are shown in Figs. 9(a) and 9(b). In these data, again strongly dispersing states crossing the Fermi energy are observed in both directions.

Since the $Dy_3Si_5/Si(111)$ multilayer forms a $\sqrt{3} \times \sqrt{3}R30°$ superstructure with respect to the substrate, the Brillouin zone reduces by a factor of $\sqrt{3}$. This is shown in Fig. 9(d), where the dashed hexagons mark the Brillouin zone of the silicide and the solid one the Brillouin zone of the substrate. The symmetry points $\bar{\Gamma}'_{111}$, $\bar{M}'_{111}$, and $\bar{K}'_{111}$ are now related to $Dy_3Si_5$, and some of them match with $\bar{\Gamma}_{111}$, $\bar{M}_{111}$, and $\bar{K}_{111}$ from the $1\times1$ reconstructed $DySi_2$ because of zone folding effects.

In Fig. 9(c), previous ARPES results on the electronic structure of $Er_3Si_5/Si(111)$ multilayers[28] are shown, characterized by two bands in the binding-energy range up to 0.8 eV. In order to compare these states with the present data, Figs. 9(e) and 9(f) show an amplification of the ARPES data in the region of low binding energies.

The electronlike parabola reported at low binding energies around $\bar{M}'_{111}$ for $Er_3Si_5/Si(111)$ is also found in the present data, as indicated by marker 1 and the red curves in Figs. 9(e) and 9(f). However, the band is only observed clearly at those $\bar{M}'_{111}$ points matching with $\bar{M}_{111}$ (marker 1), while it cannot be detected at the other $\bar{M}'_{111}$ points at marker 5. This behavior indicates that zone folding effects, which are due to scattering at the defective silicon sheets in the silicide bulk, do not play a significant role in the present ARPES experiments. This effect can be related to the high surface sensitivity at $h\nu=41$ eV and further supports the view that the states close to the Fermi energy are more related to the rare earth atoms.[29] From the parabolas at the $\bar{M}'_{111}$ points, an effective mass of about $0.5m_e$ is derived, similar to the monolayer case.

The second band at slightly higher binding energies reported in Ref. 28 is also found in the ARPES data taken in both directions, as marked by red lines in Figs. 9(e) and 9(f). Parallel to the nanowires, a wavy structure is observed, which nicely matches the $Er_3Si_5/Si(111)$ bands at markers 2, 3, and 6, as shown in Fig. 9(e). In perpendicular direction, the W-shaped curve around $\bar{M}_{111}$ is clearly observed, as indicated by markers 2, 3, and 4 in Fig. 9(f). These findings confirm the assumption that $Dy_3Si_5$ multilayers grow on the (111) facets of the Si(557) surface.

However, besides the features characteristic for $Dy_3Si_5/Si(111)$ multilayers, marked by red lines, also other

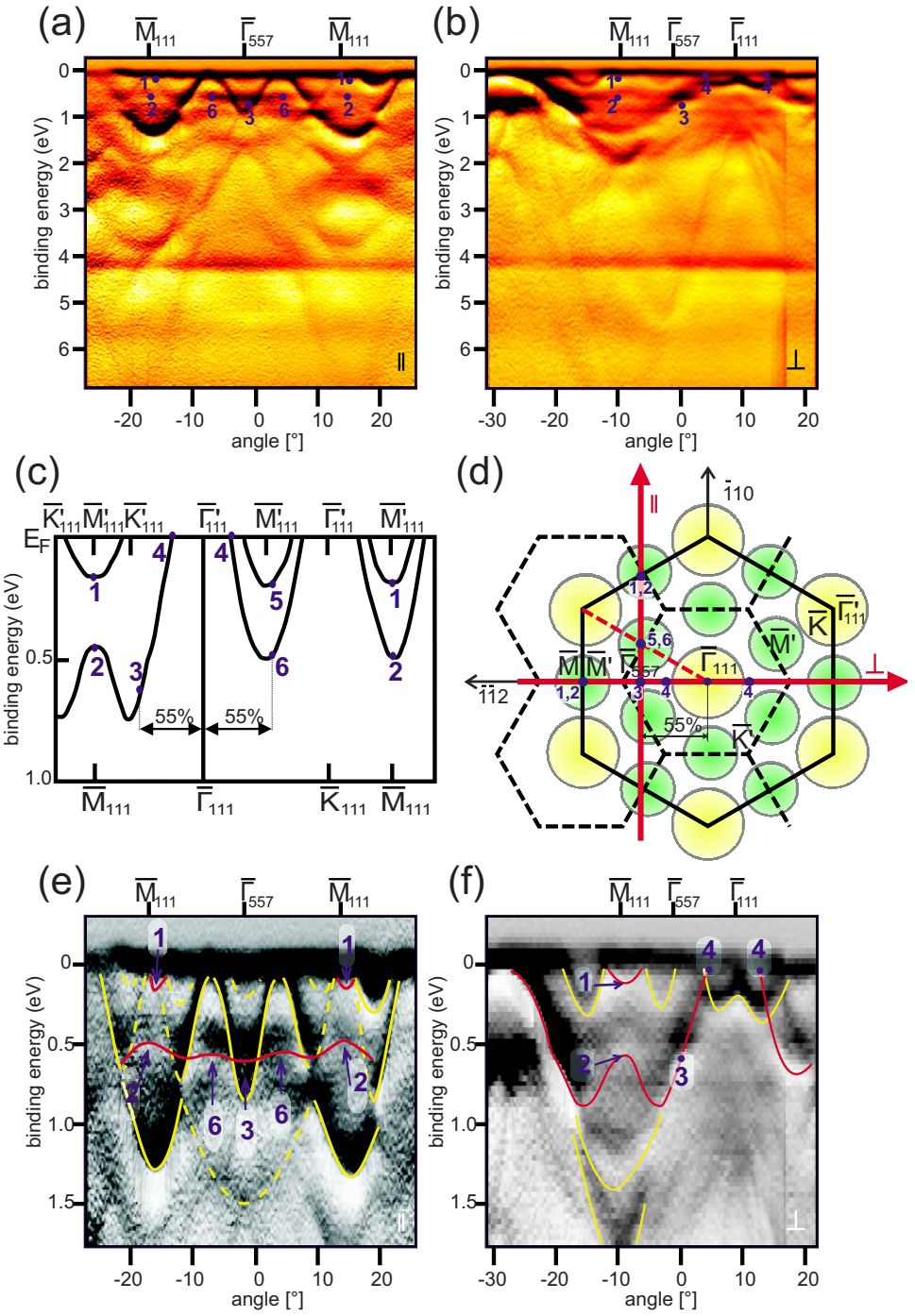


FIG. 9. (Color online) ARPES data (a) along and (b) perpendicular to the $Dy_3Si_5$ nanowires prepared with 3 Å Dy and an annealing temperature of 700 °C. The horizontal lines at around 4.3 and 5.4 eV binding energy stem from the Dy-4*f* emission. (c) Band structure of $Er_3Si_5$ on Si(111) from Ref. 28 for comparison. (d) Surface Brillouin zone of $Dy_3Si_5$ showing the directions of the measurements by red arrows. Images (e) and (f) show respective details of (a) and (b) at low binding energies, with the contributions from $Dy_3Si_5$/Si(111) marked red and those from another unknown structure marked yellow.

rather intense bands are found, which are marked yellow in Figs. 9(e) and 9(f). In Fig. 9(f), they might have the same symmetry around $\bar{\Gamma}_{111}$ so that they could be related to additional structures on the (111) facets. From the present data, however, these bands cannot be assigned to a specific structure.

It should be noted that ARPES data from the $Dy_3Si_5$ multilayer nanowires were taken within this study only at dysprosium exposures up to 3 Å. Thus the coexistence of $Dy_3Si_5$ nanowires with an additional unidentified structure can be due to nonideal sample preparation conditions. At present, it may only be speculated that higher dysprosium coverages lead to more homogeneous samples with dominating $Dy_3Si_5$ nanowires.

### E. Erbium silicide nanowires

Erbium was found to form essentially similar silicide nanowire structures on the Si(557) surface as dysprosium. As an example, the STM image in Fig. 10(a) shows mainly $ErSi_2$ monolayer nanowires with the characteristic hexagonal endpieces (dotted lines) already known from $DySi_2$. In addition, linear and chainlike structures typical for submonolayer nanowires are occasionally visible in between the monolayer nanowires.

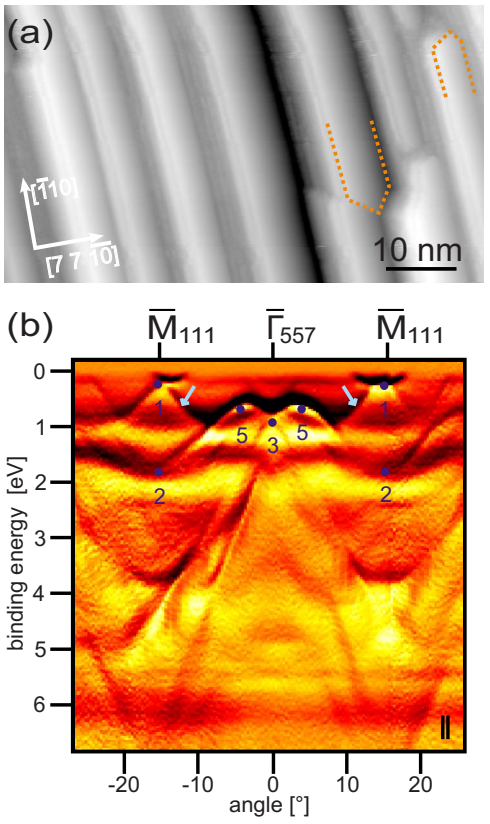


FIG. 10. (Color online) (a) STM image of $ErSi_2$ nanowires on Si(557) prepared with 2 Å Er and an annealing temperature of 700 °C. The dotted line indicates the endpieces of the nanowires with hexagonal shape characteristic for $ErSi_2$ monolayers on Si(111). (b) Corresponding ARPES data along the erbium silicide nanowires. The blue markers are related to those in Fig. 7.

This structural finding is supported by the ARPES measurements displayed in Fig. 10(b). The dominating features are the bands typical for the $ErSi_2$ monolayer, as indicated by the blue markers, which match exactly the bands of the $DySi_2$ monolayer. Less intense features from half-metallic submonolayer nanowires are also observed, as indicated by arrows, demonstrating that also very similar submonolayer structures are formed.

Generally it has been found more difficult to prepare pure $ErSi_2$ nanowires without additional $Er_3Si_5$ nanowires or submonolayer structures. This might be due to the fact that the annealing temperature for the $ErSi_2$ nanowires is about 50 °C higher than for the case of $DySi_2$ nanowires so that the parameter range for the preparation of homogeneous samples seems to be more limited.

## IV. DIMENSIONALITY OF THE ELECTRONIC STRUCTURE

In this work it has been demonstrated that for submonolayer coverages of dysprosium or erbium, only a dispersion parallel to the nanowires was observed, while there is no dispersion perpendicular to the nanowires. Such a behavior is expected for nanowire structures with widths on an atomic scale and a negligible coupling to neighboring nanowires since here a one-dimensional electronic structure develops.

In contrast, the $DySi_2$ or $ErSi_2$ monolayer nanowires as well as the $Dy_3Si_5$ or $Er_3Si_5$ multilayer nanowires are characterized by a two-dimensional electronic structure with hexagonal symmetry. Such a behavior is also expected since the width of the nanowires amounts to 3–5 nm and thus to 10 unit cells or more so that quantum size effects do not play a significant role and are—within the present experimental accuracy—not observed in the ARPES data.

Interestingly, the two-dimensional electronic structure of $DySi_2$ or $ErSi_2$ nanowires, grown on Si(557), is in strong contrast to the one-dimensional electronic structure of the so-called broad rare earth silicide nanowires grown on Si(001),[5,6] although they are formed from the same chemical compound, hexagonal rare earth disilicide. The main difference is that for the silicides on Si(557) the hexagonal *c* axis lies vertical to the (111) facets, while it lies within the substrate surface for the case of Si(001). Because of the layered structure of the silicide, the electronic coupling between neighboring rare earth layers is significantly lower than within the layers. This explains why a one-dimensional electronic structure is observed for disilicide nanowires on Si(001).

However, there are several similarities of the band structure in both nanowire systems: If the electronlike bands at the $\bar{M}_{111}$ points are projected in $\bar{\Gamma}_{111}-\bar{M}_{111}$ direction [see Fig. 7(d)], which corresponds to the [001] direction of the Si(001) substrate, similar parabolic bands are expected in the direction of the broad nanowires on Si(001). Indeed, such bands were observed for $DySi_2$ nanowires at the $\bar{\Gamma}_{001}$ and $\bar{J}_{001}$ points,[5] and a similar behavior was found for $GdSi_2$ nanowires, where they were only observed at the $\bar{J}_{001}$ point.[6] Thus the different dimensionalities found for nominally the same compound can be related to the different *c*-axis orientations.

## V. SUMMARY

In summary we presented STM and ARPES results on the formation, atomic structure, and electronic properties of self-organized dysprosium and erbium silicide nanowires on the Si(557) surface. Depending on the preparation conditions different nanowire types with different structural and electronic properties were found.

For submonolayer coverages, thin linear and chainlike structures were observed on facets tilted by about −2° relative to the (557) surface, characterized by a one-dimensional half-metallic electronic structure. The other facets with a tilt angle of about 10° were found to be (111) oriented, either with the $7\times7$ reconstruction of pure silicon or with the $2\sqrt{3}\times2\sqrt{3}$ superstructure of a rare earth submonolayer silicide.

For monolayer and multilayer coverages, broader nanowires are forming mainly on the (111) facets, with lengths even exceeding 1000 nm in some cases. They show a two-dimensional metallic dispersion of the electronic states with electronlike and holelike bands crossing the Fermi energy. From both structural and electronic data it was demonstrated that these nanowires consist of silicides already known to

grow on the Si(111) surface. For monolayer coverages, the nanowires consist of hexagonal $DySi_2$ or $ErSi_2$, and for multilayer coverages of the similar $Dy_3Si_5$ or $Er_3Si_5$ compounds. Because of the good lattice match of these silicides, the self-organized nanowire formation is related to the step structure of the substrate, in this way limiting the nanowire width.

The two-dimensional electronic structure observed for broad nanowires on Si(557) was found to be in contrast to the one-dimensional electronic structure of similar nanowires forming on Si(001), despite of the same material, hexagonal $DySi_2$ or $ErSi_2$. This effect could be related to the different *c*-axis orientations in both cases.

## ACKNOWLEDGMENTS

This work was supported by the Deutsche Forschungsgemeinschaft under Project No. Da408/11. The authors would like to acknowledge E. Weschke and G. Kaindl for providing the ARPES chamber and BESSY GmbH for providing the beamtime.

*daehne@physik.tu-berlin.de

[1] C. Preinesberger, S. Vandré, T. Kalka, and M. Dähne-Prietsch, J. Phys. D **31**, L43 (1998).
[2] J. Nogami, B. Z. Liu, M. V. Katkov, C. Ohbuchi, and N. O. Birge, Phys. Rev. B **63**, 233305 (2001).
[3] C. Preinesberger, S. K. Becker, S. Vandré, T. Kalka, and M. Dähne, J. Appl. Phys. **91**, 1695 (2002).
[4] Y. Chen, D. A. A. Ohlberg, G. Medeiros-Ribeiro, Y. A. Chang, and R. S. Williams, Appl. Phys. A: Mater. Sci. Process. **75**, 353 (2002).
[5] C. Preinesberger, G. Pruskil, S. K. Becker, M. Dähne, D. V. Vyalikh, S. L. Molodtsov, C. Laubschat, and F. Schiller, Appl. Phys. Lett. **87**, 083107 (2005).
[6] H. W. Yeom, Y. K. Kim, E. Y. Lee, K.-D. Ryang, and P. G. Kang, Phys. Rev. Lett. **95**, 205504 (2005).
[7] A. Pratt, C. Woffinden, C. Bonet, and S. Tear, Phys. Rev. B **78**, 155430 (2008).
[8] J. Zhang, M. A. Crimp, Y. Cui, and J. Nogami, J. Appl. Phys. **103**, 064308 (2008).
[9] J. A. Knapp and S. T. Picraux, Appl. Phys. Lett. **48**, 466 (1986).
[10] S. Vandré, T. Kalka, C. Preinesberger, and M. Dähne-Prietsch, Phys. Rev. Lett. **82**, 1927 (1999).
[11] S. Vandré, C. Preinesberger, T. Kalka, and M. Dähne-Prietsch, J. Vac. Sci. Technol. B **17**, 1682 (1999).
[12] S. Vandré, C. Preinesberger, W. Busse, and M. Dähne, Appl. Phys. Lett. **78**, 2012 (2001).
[13] I. Engelhardt, C. Preinesberger, S. K. Becker, H. Eisele, and M. Dähne, Surf. Sci. **600**, 755 (2006).
[14] P. Wetzel, C. Pirri, P. Paki, J. C. Peruchetti, D. Bolmont, and G. Gewinner, Solid State Commun. **82**, 235 (1992).
[15] L. Stauffer, A. Mharchi, C. Pirri, P. Wetzel, D. Bolmont, G. Gewinner, and C. Minot, Phys. Rev. B **47**, 10555 (1993).
[16] Z. He, D. J. Smith, and P. A. Bennett, Appl. Phys. Lett. **86**, 143110 (2005).
[17] A. Kirakosian, R. Bennewitz, J. N. Crain, T. Fauster, J.-L. Lin, D. Y. Petrovykh, and F. J. Himpsel, Appl. Phys. Lett. **79**, 1608 (2001).
[18] S. A. Teys, K. N. Romanyuk, R. A. Zhachuk, and B. Z. Olshanetsky, Surf. Sci. **600**, 4878 (2006).
[19] D.-H. Oh, M. K. Kim, J. H. Nam, I. Song, C.-Y. Park, S. H. Woo, H.-N. Hwang, C. C. Hwang, and J. R. Ahn, Phys. Rev. B **77**, 155430 (2008).
[20] I. K. Robinson, P. A. Bennett, and F. J. Himpsel, Phys. Rev. Lett. **88**, 096104 (2002).
[21] J. N. Crain, A. Kirakosian, K. N. Altmann, C. Bromberger, S. C. Erwin, J. L. McChesney, J.-L. Lin, and F. J. Himpsel, Phys. Rev. Lett. **90**, 176805 (2003).
[22] J. N. Crain, J. L. McChesney, F. Zheng, M. C. Gallagher, P. C. Snijders, M. Bissen, C. Gundelach, S. C. Erwin, and F. J. Himpsel, Phys. Rev. B **69**, 125401 (2004).
[23] C. Tegenkamp, Z. Kallassy, H. Pfnür, H.-L. Günter, V. Zielasek, and M. Henzler, Phys. Rev. Lett. **95**, 176804 (2005).
[24] M. Wanke, K. Löser, G. Pruskil, and M. Dähne, J. Appl. Phys. **103**, 094319 (2008).
[25] R. I. G. Uhrberg, G. V. Hansson, J. M. Nicholls, P. E. S. Persson, and S. A. Flodström, Phys. Rev. B **31**, 3805 (1985).
[26] C. Preinesberger, S. K. Becker, and M. Dähne, AIP Conf. Proc. **696**, 837 (2003).
[27] B. Z. Liu and J. Nogami, Surf. Sci. **540**, 136 (2003).
[28] P. Wetzel, S. Saintenoy, C. Pirri, D. Bolmont, and G. Gewinner, Phys. Rev. B **50**, 10886 (1994).
[29] L. Stauffer, C. Pirri, P. Wetzel, A. Mharchi, P. Paki, D. Bolmont, G. Gewinner, and C. Minot, Phys. Rev. B **46**, 13201 (1992).